Thermal management of the central processing unit cooling system using a cylindrical metal foam heat sink under the influence of magnetohydrodynamic nanofluid flow

Received 11 April 2023
Revised 8 August 2023
9 August 2023
Accepted 10 August 2023

Ali Akbar Izadi
School of Mechanical Engineering, Iran University of Science and Technology, Tehran, Islamic Republic of Iran, and

Hamed Rasam
Energy Department, Politecnico di Torino, Turin, Italy

Abstract

Purpose – Efficient thermal management of central processing unit (CPU) cooling systems is vital in the context of advancing information technology and the demand for enhanced data processing speeds. This study aims to explore the thermal performance of a CPU cooling setup using a cylindrical porous metal foam heat sink.

Design/methodology/approach – Nanofluid flow through the metal foam is simulated using the Darcy–Brinkman–Forschheimer equation, accounting for magnetic field effects. The temperature distribution is modeled through the local thermal equilibrium equation, considering viscous dissipation. The problem's governing partial differential equations are solved using the similarity method. The CPU's hot surface serves as a solid wall, with nanofluid entering the heat sink as an impinging jet. Verification of the numerical results involves comparison with existing research, demonstrating strong agreement across numerical, analytical and experimental findings. Ansys Fluent® software is used to assess temperature, velocity and streamlines, yielding satisfactory results from an engineering standpoint.

Findings – Investigating critical parameters such as Darcy number ($10^{-4} \leq Da_D \leq 10^{-2}$), aspect ratio ($0.5 \leq H/D \leq 1.5$), Reynolds number ($5 \leq Re_{D,bf} \leq 3500$), Eckert number ($0 \leq EC_{bf} \leq 0.1$) , porosity ($0.85 \leq \varepsilon \leq 0.95$), Hartmann number ($0 \leq Ha_{D,bf} \leq 300$) and the volume fraction of nanofluid ($0 \leq \varphi \leq 0.1$) reveals their impact on fluid flow and heat sink performance. Notably, Nusselt number will reduce 45%, rise 19.2%, decrease 14.1%, and decrease 0.15% for Reynolds numbers of 600, with rising porosity from 0.85 to 0.95, Darcy numbers from 10^{-4} to 10^{-2}, Eckert numbers from 0 to 0.1, and Hartman numbers from 0 to 300.

Originality/value – Despite notable progress in studying thermal management in CPU cooling systems using porous media and nanofluids, there are still significant gaps in the existing literature. First, few studies have considered the Darcy–Brinkman–Forchheimer equation, which accounts for non-Darcy effects and the flow and geometric interactions between coolant and porous medium. The influence of viscous dissipation on heat transfer in this specific geometry has also been largely overlooked. Additionally, while nanofluids and impinging jets have demonstrated potential in enhancing thermal performance, their utilization within porous media

International Journal of Numerical Methods for Heat & Fluid Flow
Vol. 34 No. 1, 2024
pp. 1-30
Emerald Publishing Limited
0961-5539
DOI 10.1108/HFF-04-2023-0188

remains underexplored. Furthermore, the unique thermal and structural characteristics of porous media, along with the incorporation of a magnetic field, have not been fully investigated in this particular configuration. Consequently, this study aims to address these literature gaps and introduce novel advancements in analytical modeling, non-Darcy flow, viscous dissipation, nanofluid utilization, impinging jets, porous media characteristics and the impact of a magnetic field. These contributions hold promising prospects for improving CPU cooling system thermal management and have broader implications across various applications in the field.

Keywords CPU cooling, Nanofluid, Magnetohydrodynamics, Similarity solution, Viscous dissipation

Paper type Research paper

Nomenclature

B = Magnetic field (T);
Ec = Eckert number;
C_E = Form drag coefficient;
c_p = Specific heat (J/kg.K);
D = Diameter of heat sink;
Da = Darcy number;
f(Y) = Similarity functions;
H = Height of heat sink (m);
Ha = Hartmann number;
k = Thermal conductivity (W/m.K);
K = Permeability (m^2);
Nu = Nusselt number;
p = Pressure (Pa);
P = Dimensionless pressure;
Pr = Prandtl number;
Re = Reynolds number;
T = Temperature (K);
T_{inlet} = Inlet temperature (K); and
T_w = Wall temperature (K).

Superscripts

$', '', ''', iv$ = First, Second, Third and Fourth derivatives;
u_r, u_z = Radial-Axial velocity (m/s);
V_{jet} = Average jet velocity (m/s); and
r, z = Cylindrical coordinates.

Greek symbols

ε = Porosity;
σ = Electrical conductivity $(\Omega m)^{-1}$;
φ = Nanoparticle volume fraction;
ψ = Stream function;
Φ = Viscous dissipation term;
μ = Dynamic viscosity (Pa.s);
η = Similarity parameter;
ϑ = Kinematic viscosity (m^2/s);
θ = Dimensionless temperature; and
ρ = Density (kg/m^3).

Subscripts
bf = Base fluid;
eff = Effective;
nf = Nanofluid;
np = Nanoparticle;
s = Solid phase; and
0 = Initial amount.

1. Introduction

The heat sink plays a pivotal role in maintaining stable temperatures within central processing units (CPUs), serving as a passive heat exchanger that adeptly absorbs a substantial amount of heat without inducing significant changes in temperature. Such heat exchanger designs find widespread utilization in various industrial applications (Liu and Garimella, 2005). One of its most prevalent and unique applications is in electrical and computer equipment (Rasam *et al.*, 2020), like CPUs (Naphon *et al.*, 2009). Heat sinks, characterized by their high porosity, accelerated CPU processing speed after maintaining this unit's temperature constant. Engineers had to use CPUs with minuscule sizes to meet the growing need for compacting the size of electronic gadgets, thereby reducing the size of heat sinks (Choi *et al.*, 2012). In a similar vein, using open-cell metal foam with high porosity in place of fins compacts the heat sinks while also increasing the surface area in contact with the cooling liquid (Odabaee *et al.*, 2013). Despite its small size, an open-cell metal foam heat sink dissipates more heat from the CPU (Gorzin *et al.*, 2022). However, it can be difficult to maximize the dissipation of accumulated heat in the processing unit due to several restrictions, such as the small size of electronic devices, typical materials and existing procedures.

A method for enhancing heat sink performance is to use nanofluid as the cooling fluid (Goodarzi *et al.*, 2019). Nanofluids entail the incorporation of minuscule particles into conventional fluids, such as water, to amplify the cooling fluid's thermal conductivity (Rezazad Bari *et al.*, 2023). This approach holds promise for elevating the heat transfer rate within CPUs (Bahiraei and Heshmatian, 2017). As an illustration, Nazari *et al.* (2014) experimentally tested the effectiveness of several nanofluids with one another and with other base fluids, such as water and ethylene glycol, in experimental work for cooling CPU. The CNT nanofluid with a volume fraction of 0.25% reportedly had the best thermal performance, according to their analysis. In a different study, Al-Rashed *et al.* (2016) used experimental and numerical comparisons to assess the cooling performance of CuO nanofluid with pure water for CPUs. Their research showed that, when compared to pure water, the thermal performance of nanofluids might be improved by 7.7%. As a result, the employment of nanofluid as a supplement to porous media has drawn a large number of researchers to this strategy for improving the performance of compact 21st century CPUs. However, because the behavior of nanofluids via porous media is complex, the employment of this technique is far from the end of science and technological progress for the final maximizing of thermal efficiency (Khan *et al.*, 2013). Therefore, additional study in this area is still necessary.

Considerable efforts, hitherto, have been devoted to studying the heat and mass transfer of nanofluid inside open-cell metal foam heat sinks. In this regard, Hajipour and Molaei Dehkordi (Hajipour and Dehkordi, 2012) investigated nanofluid mixed convective inside a channel filled with porous metal foam by experimental and numerical research. According to empirical findings, using nanofluid with a concentration of 0.3% increases heat transfer rate by 20% when compared to distilled water. The addition of nanoparticles to pure water

has no appreciable impact, and the highest pressure decrease is only about 5%. With a maximum variance of 8.6%, the numerical results and experimental data match up well. Another investigation was conducted by Xu *et al.* (2015) to examine the temperature and flow characteristics of nanofluid and forced convection inside a duct filled with porous media. The findings demonstrate that porosity has an increasing relation with pressure drop and Nusselt number. Our understanding of the thermal characteristics of a nanofluid through an open-cell metal foam heat sink has significantly increased as a result of prior investigations. These investigations will significantly facilitate the advancement of science and technology in the near future. Nevertheless, there are frequently numerous critical aspects involved in an ordinary subject of heat and mass transfer within an open-cell metal foam heat sink, which is still too expensive to analyze empirically and numerically in a parametric examination. To initially have a main approximation, the majority of the problems demand a timely and expensive effective solution with accurate results; as a result, an experimental and numerical solution as an exact simulation might be applied (Mohebbi and Rasam, 2020). Therefore, a quick, low-cost seminumerical or analytical method with a trustworthy prediction is needed to make adequate development in the field of heat and mass transfer of nanofluid within an open-cell metal foam.

A prominent classification for partial differential equations (PDE) solving is similarity solutions, which have a broad range of applications in the fields of fluid dynamics and thermal research (Sheikholeslami and Ganji, 2016). Recent studies have examined the thermal behavior of nanofluids through porous media using this technique using both local thermal equilibrium (Siavashi *et al.*, 2019) and local thermal nonequilibrium (LTNE) (Izadi *et al.*, 2020a) energy equation models. For instance, Nield and Kuznetsov (2009) studied free convection heat transfer on a vertical plate in a porous medium saturated with nanofluid using a similarity solution. Their findings include analyses of how important variables such as the Lewis number, buoyancy-ratio number and others affect the Nusselt number, an indicator of thermal performance. In another semi-analytical study, Izadi *et al.* (2019) used a similarity solution to investigate the flow and thermal performance of a porous heat sink cooling with nanofluid. Having chosen the appropriate similarity variable, they were able to convert the PDE that appeared from the energy and momentum solution to an ordinary differential equation (ODE). According to these investigations, authors, using similarity solutions is an effective way to anticipate the problem's justified results. As a result, the similarity solution has been used in this study to examine the thermal behavior of nanofluid flow inside a porous heat sink. However, it is noteworthy that the influence of viscous dissipation, which makes the behavior of nanofluid inside a cylindrical porous heat sink more realistic, has not yet been used with applying similarity solutions. For this purpose, recent research strengthens the similarity method's current ability to increase precision by taking viscous dissipation into account.

The field of magnetohydrodynamics (MHD) explores the behavior of conductive fluids in the presence of magnetic body forces (Aly and Pop, 2019). The literature on the topic claims that magnetic force could either have a beneficial or adverse effect on heat transfer in different geometry such as curved channel (Iqbal *et al.*, 2023), flat plate (Reddy and Goud, 2023), trapezoidal microchannel (Sepehrnia *et al.*, 2021) and square cavity (Geridönmez and Öztop, 2021). Numerous studies have documented the enhancement of heat transfer caused by the influence of a magnetic field on a nanofluid used as a coolant in a porous heat sink (Izadi *et al.*, 2020b). In similar vein, Hosseini and Sheikholeslami (2019) investigated the influence of a magnetic field on nanofluid cooling of a microchannel heat sink in a numerical

study. Their final results demonstrated how the thermal performance will be directly impacted by applying a magnetic field. They stated that the increase in momentum in the area adjacent to the wall is the result of the concentration of nanofluid. Sheikholeslami (2018) examined numerically the influence of MHD on fluid-forced convection by using LBM. According to the findings, the velocity field, temperature distribution and Nusselt number are all greatly affected by magnetic force. The aforementioned studies have shown that magnetic force will undoubtedly accelerate the flow of nanofluid in porous medium. However, many of these studies in this area have been performed using numerical and experimental methods (Akbar and Khan, 2015). An analytical investigation on MHD of nanofluid through a porous cylindrical metal heat sink is therefore considered essential.

Despite notable progress in studying thermal management in CPU cooling systems using porous media and nanofluids, there are still significant gaps in the existing literature. First, few studies have considered the Darcy–Brinkman–Forchheimer equation, which accounts for non-Darcy effects and the flow and geometric interactions between coolant and porous medium. The influence of viscous dissipation on heat transfer in this specific geometry has also been largely overlooked. Additionally, while nanofluids and impinging jets have demonstrated potential in enhancing thermal performance, their utilization within porous media remains underexplored. Furthermore, the unique thermal and structural characteristics of porous media, along with the incorporation of a magnetic field, have not been fully investigated in this particular configuration. Consequently, this study aims to address these literature gaps and introduce novel advancements in analytical modeling, non-Darcy flow, viscous dissipation, nanofluid utilization, impinging jets, porous media characteristics and the impact of a magnetic field. These contributions hold promising prospects for improving CPU cooling system thermal management and have broader implications across various applications in the field.

2. Problem statement

A recent problem scrutinizes an open-cell metal foam heat sink with high porosity exposed to a uniform cooling fluid. The cooling fluid, which is specifically nanofluid, enters the heat sink with V_{inlet} velocity and T_{inlet} temperature and after the cooling process, it would exit from the sides. The temperature of heat sink bed is constant and equal to T_w, which is always $T_w > T_{inlet}$. In this problem, the assumption of thermal equilibrium between cooling fluid and porous media has been applied. The fluid flow through the porous media is steady, Newtonian and laminar. The effect of gravitation is neglected, while the effects of viscous dissipation have been considered. The solid phase is rigid, homogenous and isotropic. In addition, the solid- and fluid-phases properties are constant with respect to the temperature, and a uniform magnetic field affects the heat sink. From the geometry aspect, the diameter and height are D and H, respectively. According to the physics of the problem, the computation domain has been assumed to be two-dimensional (Mahesh *et al.*, 2023; Hussain and Sheremet, 2023; Huang *et al.*, 2010) (Figure 1).

3. Governing equations

In accordance with assumptions, the conservation equations of mass, momentum and energy could be stated as follows (Huang *et al.*, 2010; Mohamad, 2003; Pavel and Mohamad, 2004):

$$\frac{1}{r}\frac{\partial}{\partial r}(ru_r) + \frac{\partial u_z}{\partial z} = 0 \tag{1}$$

$$\frac{1}{\varepsilon^2}\left(u_r\frac{\partial u_r}{\partial r}+u_z\frac{\partial u_r}{\partial z}\right)=-\frac{1}{\rho_{nf}}\frac{\partial p}{\partial r}+\frac{\vartheta_{nf}}{\varepsilon}\left[\frac{1}{r}\frac{\partial}{\partial r}\left(r\frac{\partial u_r}{\partial r}\right)+\frac{\partial^2 u_r}{\partial z^2}-\frac{u_r}{r^2}\right]-\frac{\vartheta_{nf}}{K}u_r$$
$$-\frac{C_E}{\sqrt{K}}\left(\sqrt{{u_r}^2+{u_z}^2}\right)u_r-\left(\frac{\sigma}{\rho}\right)_{nf}B_0^2u_r \tag{2}$$

$$\frac{1}{\varepsilon^2}\left(u_r\frac{\partial u_z}{\partial r}+u_z\frac{\partial u_z}{\partial z}\right)=-\frac{1}{\rho_{nf}}\frac{\partial p}{\partial z}+\frac{\vartheta_{nf}}{\varepsilon}\left[\frac{1}{r}\frac{\partial}{\partial r}\left(r\frac{\partial u_z}{\partial r}\right)+\frac{\partial^2 u_z}{\partial z^2}\right]-\frac{\vartheta_{nf}}{K}u_z$$
$$-\frac{C_E}{\sqrt{K}}\left(\sqrt{{u_r}^2+{u_z}^2}\right)u_z \tag{3}$$

$$(\rho c_p)_{nf}\left(u_r\frac{\partial T}{\partial r}+u_z\frac{\partial T}{\partial z}\right)=k_{eff}\left(\frac{1}{r}\frac{\partial}{\partial r}\left(r\frac{\partial T}{\partial r}\right)+\frac{\partial^2 T}{\partial z^2}\right)+\Phi \tag{4}$$

in which Φ viscous dissipation term is defined as (Dhahri *et al.*, 2010):

$$\Phi=\frac{\mu_{nf}}{k}\left(u_r^2+u_z^2\right)+\frac{\mu_{nf}}{\varepsilon}\left[2\left\{\left(\frac{\partial u_r}{\partial r}\right)^2+\left(\frac{u_r}{r}\right)^2+\left(\frac{\partial u_z}{\partial z}\right)^2\right\}+\left(\frac{\partial u_r}{\partial z}+\frac{\partial u_z}{\partial r}\right)^2\right] \tag{5}$$

and the effective thermal conductivity would be defined as:

$$k_{eff}=\varepsilon k_{nf}+(1-\varepsilon)k_s \tag{6}$$

the boundary conditions governing the problem are expressed as:

$$u_r=0,\ u_z=0,\quad T=T_w \qquad z=0 \tag{7}$$

$$u_r=0,\ u_z=-V_{inlet},\quad T=T_{inlet} \qquad z=H \tag{8}$$

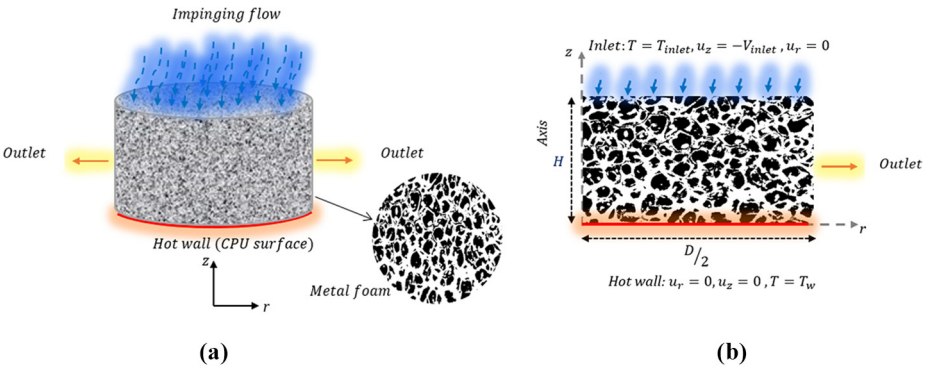

Figure 1.
Schematic of the problem geometry (a) 3D geometry of metal foam and (b) 2D geometry and boundary conditions

Source: Figure by authors

4. Similarity solution

In this section, to clarify the solution procedures, the similarity variables included in the analytical solution will be presented, and they will be inserted into the momentum and energy equations. According to the reference (Feng *et al.*, 2015), the momentum equations could be written as:

$$\frac{1}{r}\frac{\partial}{\partial r}(ru_r)+\frac{\partial u_z}{\partial z}=0 \tag{9}$$

$$\frac{1}{\varepsilon^2}\left(u_r\frac{\partial u_r}{\partial r}+u_z\frac{\partial u_r}{\partial z}\right)=-\frac{1}{\rho_{nf}}\frac{\partial p}{\partial r}+\frac{\vartheta_{nf}}{\varepsilon}\left[\frac{1}{r}\frac{\partial}{\partial r}\left(r\frac{\partial u_r}{\partial r}\right)+\frac{\partial^2 u_r}{\partial z^2}-\frac{u_r}{r^2}\right]-\frac{\vartheta_{nf}}{K}u_r - \frac{C_E}{\sqrt{K}}|u_r|u_r-\left(\frac{\sigma}{\rho}\right)_{nf}B_0^2u_r \tag{10}$$

$$\frac{1}{\varepsilon^2}\left(u_r\frac{\partial u_z}{\partial r}+u_z\frac{\partial u_z}{\partial z}\right)=-\frac{1}{\rho_{nf}}\frac{\partial p}{\partial z}+\frac{\vartheta_{nf}}{\varepsilon}\left[\frac{1}{r}\frac{\partial}{\partial r}\left(r\frac{\partial u_z}{\partial r}\right)+\frac{\partial^2 u_z}{\partial z^2}\right]-\frac{\vartheta_{nf}}{K}u_z-\frac{C_E}{\sqrt{K}}|u_z|u_z \tag{11}$$

With consideration of the velocity profiles and by substituting these profiles, the mass conservation equation would be satisfied, and the momentum equations would be defined simply as (Sepasgozar *et al.*, 2017):

$$\eta=\frac{z}{H},\quad \psi=V_{inlet}\frac{r^2}{2}f(\eta),\quad u_r=\frac{r}{2H}V_{inlet}f'(\eta),\quad u_z=-V_{inlet}f(\eta) \tag{12}$$

$$\frac{1}{\rho_{nf}}\frac{\partial p}{\partial r}=\frac{rV_{inlet}}{2H}\left[\frac{V_{inlet}}{2H\varepsilon^2}\left(2ff''-f'^2\right)+\frac{\vartheta_{nf}}{\varepsilon H^2}f'''-\left(\frac{\vartheta_{nf}}{k}+\left(\frac{\sigma}{\rho}\right)_{nf}B_0^2\right)f'-\frac{rV_{inlet}}{2H}\frac{C_E}{\sqrt{k}}f'^2\right] \tag{13}$$

$$-\frac{1}{\rho_{nf}}\frac{\partial p}{\partial \eta}=\left(\frac{V_{inlet}}{\varepsilon}\right)^2ff'+\frac{\vartheta_{nf}V_{inlet}}{\varepsilon H}f''-\frac{\vartheta_{nf}HV_{inlet}}{k}f-\frac{HC_EV_{inlet}^2}{\sqrt{k}}f^2 \tag{14}$$

Eventually, with the elimination of pressure from equations (13) and (14), the final form of momentum is written as:

$$f^{iv}+\left(\frac{1}{\varepsilon}\right)\left(\frac{H}{D}\right)(Re_D)ff'''-\varepsilon\left(\frac{H}{D}\right)^2\left(\frac{1}{Da_D}+Ha_D{}^2\right)f''-\varepsilon C_E\left(\frac{r}{D}\right)\left(\frac{H}{D}\right)\frac{Re_D}{\sqrt{Da_D}}f'f''=0 \tag{15}$$

$$f(0)=0,\quad f'(0)=0,\quad f(1)=1,\quad f'(1)=0 \tag{16}$$

The dimensionless numbers mentioned in the equation (15) is defined as:

$$Da_D = \frac{k}{D^2},\ Ha_D = DB_0\sqrt{\left(\frac{\sigma}{\mu}\right)_{nf}},\ Re_D = \frac{V_{inlet}D}{\vartheta_{nf}} \tag{17}$$

Likewise, with consideration of the nondimensional temperature profile as a function of the similarity variable of η placed in equation (4), the energy equation will be formed as:

$$\theta(\eta) = \frac{T - T_{inlet}}{T_w - T_{inlet}} \tag{18}$$

$$\theta'' + PrRe_D\left(\frac{H}{D}\right)f\theta' + \frac{PrEc}{Da_D}\left[\left\{\left(\frac{r}{2D}\right)^2 + 3\left(\frac{Da_D}{\varepsilon}\right)\right\}f'^2 + \left(\frac{H}{D}\right)^2 f^2 + \left(\frac{Da_D}{\varepsilon}\right)\left(\frac{r}{2D}\right)^2\left(\frac{H}{D}\right)^{-2} f''^2\right] = 0 \tag{19}$$

$$\theta(0) = 1, \quad \theta(1) = 0 \tag{20}$$

The dimensionless numbers in equation (19) are defined as:

$$Ec = \frac{V_{inlet}^2}{c_{pnf}\Delta T}, Pr = \frac{\vartheta_{nf}}{\alpha}, \alpha = \frac{k_{eff}}{(\rho c_p)_{nf}} \tag{21}$$

In the aforesaid equations, nanofluid properties are calculated as following relations. In addition, the base fluid properties and the nanoparticles' characteristics are listed in Table 1 (Khan *et al.*, 2020b):

$$\rho_{nf} = (1 - \varphi)\rho_{bf} + \varphi\rho_{np} \tag{22}$$

$$(\rho c_p)_{nf} = (1 - \varphi)(\rho c_p)_{bf} + \varphi(\rho c_p)_{np} \tag{23}$$

$$\mu_{nf} = \frac{\mu_{bf}}{(1 - \varphi)^{2.5}} \tag{24}$$

$$\frac{k_{nf}}{k_{bf}} = \frac{k_{np} + 2k_{bf} - 2\varphi(k_{bf} - k_{np})}{k_{np} + 2k_{bf} + \varphi(k_{bf} - k_{np})} \tag{25}$$

Table 1. Thermo-physical properties of base fluid and nanoparticle (Hussain *et al.*, 2016)

Material	$\rho\left(\frac{kg}{m^3}\right)$	$c_p\left(\frac{J}{kg.K}\right)$	$k\left(\frac{W}{m.K}\right)$	$\sigma(\Omega m)^{-1}$
Water	997.1	4,179	0.613	0.05
Alumina	3,970	765	40	1×10^{-10}

Source: Table by authors

$$\frac{\sigma_{nf}}{\sigma_{bf}} = 1 + \frac{3(\sigma - 1)\varphi}{(\sigma + 2) - (\sigma - 1)\varphi}, \quad \sigma = \frac{\sigma_{np}}{\sigma_{bf}} \tag{26}$$

To investigate the effects of flow, geometric and porous media nondimensional parameters on the thermal performance of the heat sink, the Nusselt number is computed as (Khan *et al.*, 2020a):

$$h = \frac{q''_{base}}{T_{base} - T_{in}} = -\frac{k_{eff}}{H}\theta'(0) \tag{27}$$

$$Nu = \frac{hD}{k_{bf}} = -\left(\frac{k_{eff}}{k_{bf}}\right)\left(\frac{D}{H}\right)\theta'(0) \tag{28}$$

$$\overline{Nu} = \frac{1}{A_{base}}\int_{A_{base}} NudA \tag{29}$$

5. Verification

The ODEs governing the flow and forced convective heat transfer of the porous heat sink have been solved numerically under the appropriate boundary conditions. To validate the outcomes obtained from the similarity solution with the assistance of the bvp4c solver of MATLAB software (Shampine *et al.*, 2000), first, the local Nusselt number was examined to confirm network independence. In the grid with 10,000 grids and the grid with 12,100 grids, the Nusselt number differs by 2.3%. For the grid with 12,100 grids and the grid with 14,400 grids, this difference is 1.23%. Additionally, the variation between the 14,400-grid and 16,900-grid grids is 0.2%. To solve the problem independently of the network, it is, therefore, decided to consider the 14,400-grid network when the difference is less than 1% [see Figure 2(a)]. Second, pressure drops as a function of flow rate were compared with the analytical and experimental work done by Do *et al.* (2010) [see Figure 2(b)]. Third, the velocity components were compared with an analytical solution (Sheikholeslami *et al.*, 2013) [see Figure 2(c)]. Fourth, having compared the velocity and temperature profiles, a verification with previous research is accomplished (Izadi *et al.*, 2019) [see Figure 2(d)]. Finally, the equations governing the problem were solved using Ansys–Fluent software with the utility of Simple algorithm (Patankar, 1980) (see Figure 3). In all cases of this broad comparison, there was acceptable agreement between the recent solution and the other methods used in previous works. The characteristics of the metal foam used in Figure 3 are shown in Table 2.

6. Results and discussions

In accordance with the verification, the similarity solution paves the way for studying the effects of nondimensional parameters on the velocity and temperature profiles and thermal performance of the system, including Reynolds number, porosity, Hartmann number, Eckert number aspect ratio of the heat sink and so forth. The results section would be divided into two parts: effects of the parameters on dimensionless velocity and temperature profiles; and the effects of parameters on Nusselt number. This point should be noted that all the parameters are constant unless otherwise specified. The list of constant parameters is given in Tables 3 and 4.

6.1 Velocity and temperature profiles

Following the pattern of fluid behavior, the impact of nondimensional numbers of Darcy, aspect ratio, Reynolds, Eckert, porosity, Hartmann and nanofluid volume fraction on the velocity and temperature profiles has been studied in this section. These numbers serve as representatives of permeability, heat sink size, momentum, viscous dissipation, porosity magnetic field and nanofluid fraction, respectively.

6.1.1 Darcy number. Figure 4 illustrates the effects of the Darcy number on the dimensionless profiles of velocity and temperature. As observed, an increase in the Darcy number leads to higher velocity profiles and lower temperature profiles. This phenomenon can be logically justified by considering the enhanced permeability of the porous media. With greater permeability, the fluid can flow more easily through the porous structure, resulting in increased velocity near the porous surface. This effect is particularly pronounced near the wall or $Y \approx 0$, where the velocity gradient decreases, consequently reducing the shear stress [see Figure 4(b)]. The Darcy number, influenced by parameters such as the pressure drop, fluid viscosity and permeability of the porous medium, plays a crucial role in determining the flow behavior. A higher Darcy number indicates a more permeable porous structure, enabling fluid to flow more freely. The relationship between the

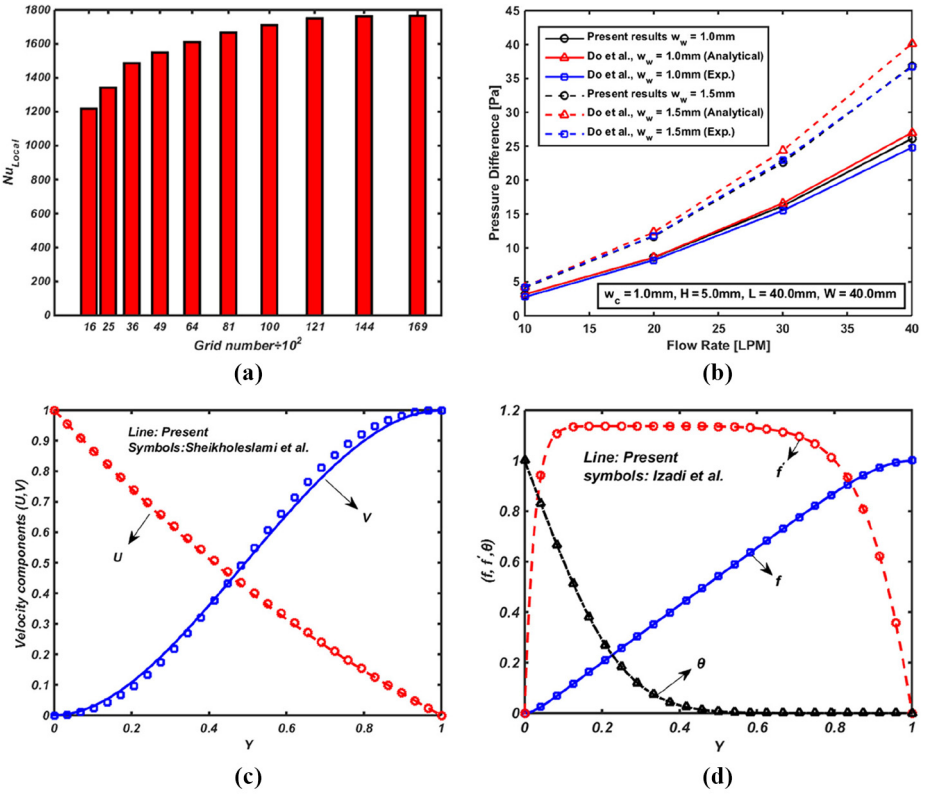

Figure 2.
(a) Grid independency analysis, (b) Comparison of the present numerical solution with analytical and experimental results for the pressure difference presented by Do *et al.* (2010), (c) comparison between present numerical solution and analytical results presented by Sheikholeslami *et al.* (2013) for ($Re = 0.5$, $Ha = 0.5$, $\varphi = 0.05$) and (d) comparison between present numerical solution and results presented by Izadi *et al.* (2019) for ($\varepsilon = 0.85$, $Da_L = 1 \times 10^{-3}$, $\varphi = 0.06$)

Source: Figure by authors

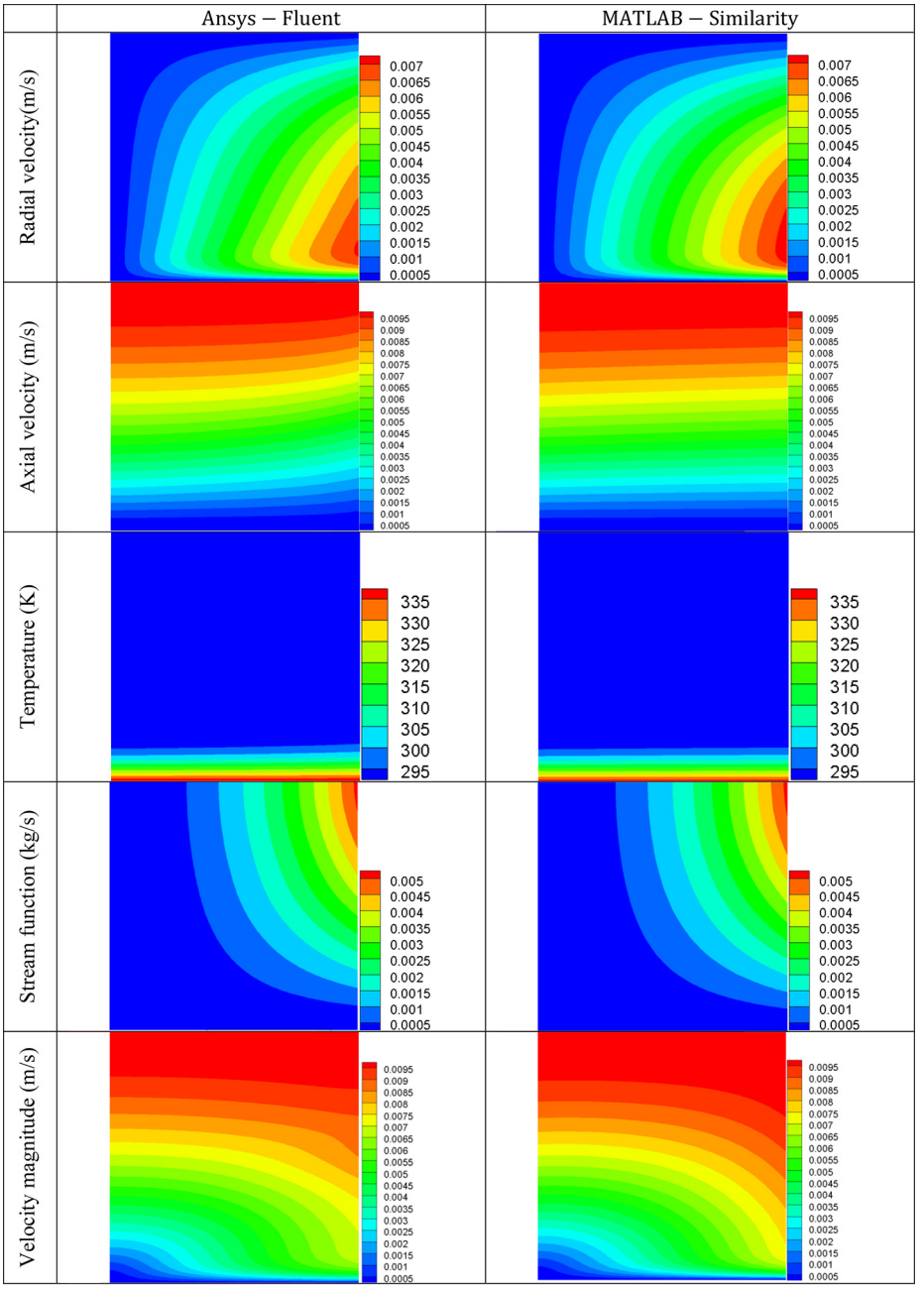

Source: Figure by authors

Figure 3.
Comparison contour of the velocity field, temperature and stream function between similarity solution and simple algorithm conducted by Ansys–Fluent software

Darcy number, velocity profiles and permeability aligns with the fundamental principles of porous media flow. Furthermore, the increased velocity field resulting from a higher Darcy number enhances the convection field, leading to more efficient cooling. The rise in the convection field contributes to a reduction in the temperature profile within the system. Therefore, as the Darcy number increases, there is a dual effect: an increase in velocity profiles and a decrease in temperature profiles. These findings, as demonstrated in Figure 4, highlight the intricate interplay between fluid flow and heat transfer in the porous cooling system.

6.1.2 Aspect ratio. In Figure 5, we examine the influence of the size ratio of the heat sink on the nondimensional profiles of velocity and temperature. The aspect ratio of the heat sink significantly affects the velocity profile. When $H < D$, where the height of the heat sink is smaller than the diameter, the cooling fluid enters the heat sink through an impinging jet, encountering less frictional resistance to reach the bottom of the heat sink. In this case, as the heat sink height decreases while maintaining a constant diameter, the outlet area of the heat sink also decreases. Consequently, at a constant mass flow rate, the velocity field within the heat sink becomes amplified. Conversely, when $H > D$, with the heat sink height taller than the diameter, the cooling fluid encounters greater frictional resistance in reaching the bottom wall. Additionally, the increased heat sink height leads to a larger outlet area. As a result, at a constant mass flow rate, the velocity field within the heat sink becomes weaker compared to the case when $H = D$ [as shown in Figure 5(b)]. The aspect ratio of the heat sink has a direct impact on thermal resistance. With an increasing aspect ratio, the overall thermal resistance of the heat sink rises. Consequently, regions farther from the hot region or $Y \approx 1$ exhibit lower temperatures [as depicted in Figure 5(c)]. The higher aspect ratio creates a longer heat transfer path, increasing the resistance to heat flow. This results in a gradual temperature decrease in regions further away from the heat source.

6.1.3 Reynolds number. Figure 6 illustrates the variations in nondimensional temperature and velocity profiles as a function of Reynolds number. The Reynolds number, defined as the ratio of inertia force to viscous force, provides valuable insights into the dominant forces governing fluid flow. An increase in the Reynolds number signifies the

Table 2. Metal foam properties (Calmidi and Mahajan, 2000)

Material	Porosity	c_E	K($\times 10^7 m^2$)	k_s(W/m.k)
Metal foam	0.9118	0.085	1.8	95

Source: Table by authors

Table 3. Constant parameters for velocity and temperature profile

Ec	ε	H/D	Re_D	C_E	r/D	Da_D	Ha_D	φ	k_s (W/m.K)
0.001	0.9	1	25	0.085	0.5	10^{-3}	30	0.05	95

Source: Table by authors

Table 4. Constant parameters for Nusselt number

Ec	ε	H/D	D(mm)	C_E	Da_D	Ha_D	φ	k_s (W/m.K)
0.01	0.9	1	60	0.085	10^{-3}	30	0.05	95

Source: Table by authors

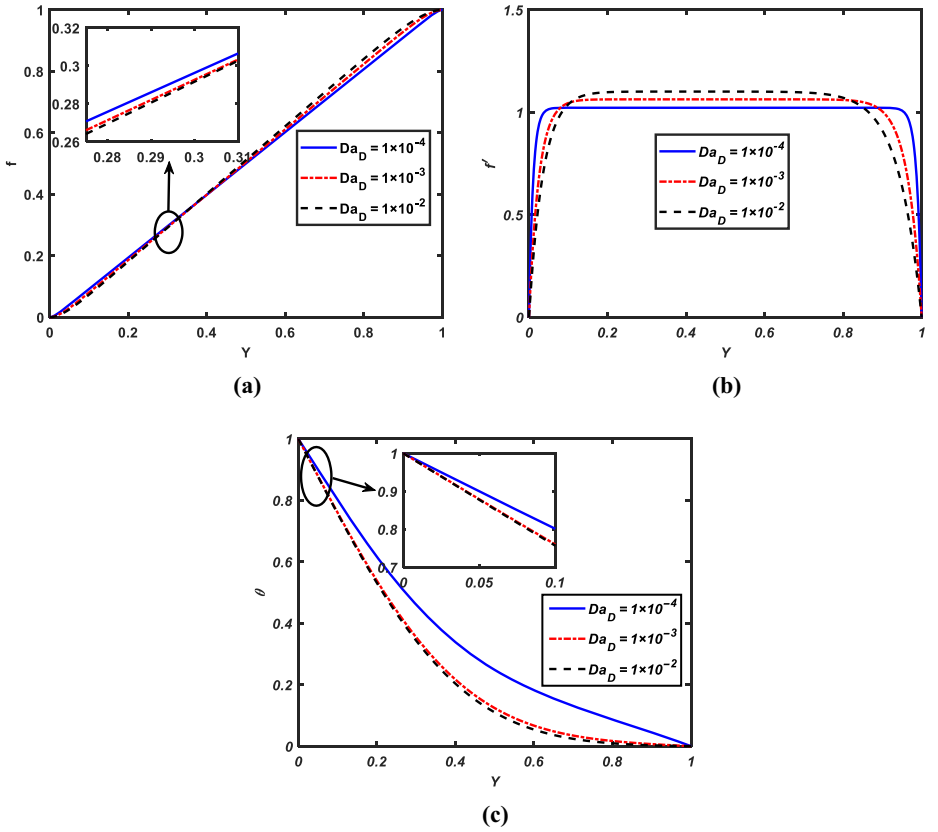

Source: Figure by authors

Figure 4.
Effect of Darcy number on: (a) f profile, (b) f' profile and (c) θ profile

growing influence of inertia forces over viscous forces. This dominance of inertia forces leads to a higher momentum of fluid flow through the porous media. Consequently, as expected, an increase in the Reynolds number amplifies the velocity field, resulting in a larger magnitude of velocities [Figure 6(a) and (b)]. As the Reynolds number rises, the velocity gradient near the wall region also increases. However, the rate of growth of shear stress slows down. This phenomenon can be attributed to the stronger influence of inertia forces that allow more fluid to reach the regions nearby the wall, reducing the velocity gradient and mitigating the growth of shear stress. Moreover, an increase in the Reynolds number enables more fluid to reach the hot areas, specifically the bottom of the heat sink. This enhanced fluid flow, accompanied by the intensification of the convection field, enhances the cooling performance. As a result, the temperature profile exhibits a noticeable decrease, indicating better heat dissipation [Figure 6(c)].

6.1.4 Eckert number. Figure 7 showcases the impact of the Eckert number on the nondimensional temperature profile. As observed in the figure, an increase in the Eckert number results in a rise in the dimensionless temperature profile. This phenomenon can be attributed to the effect of viscous dissipation, which plays a crucial role in influencing the

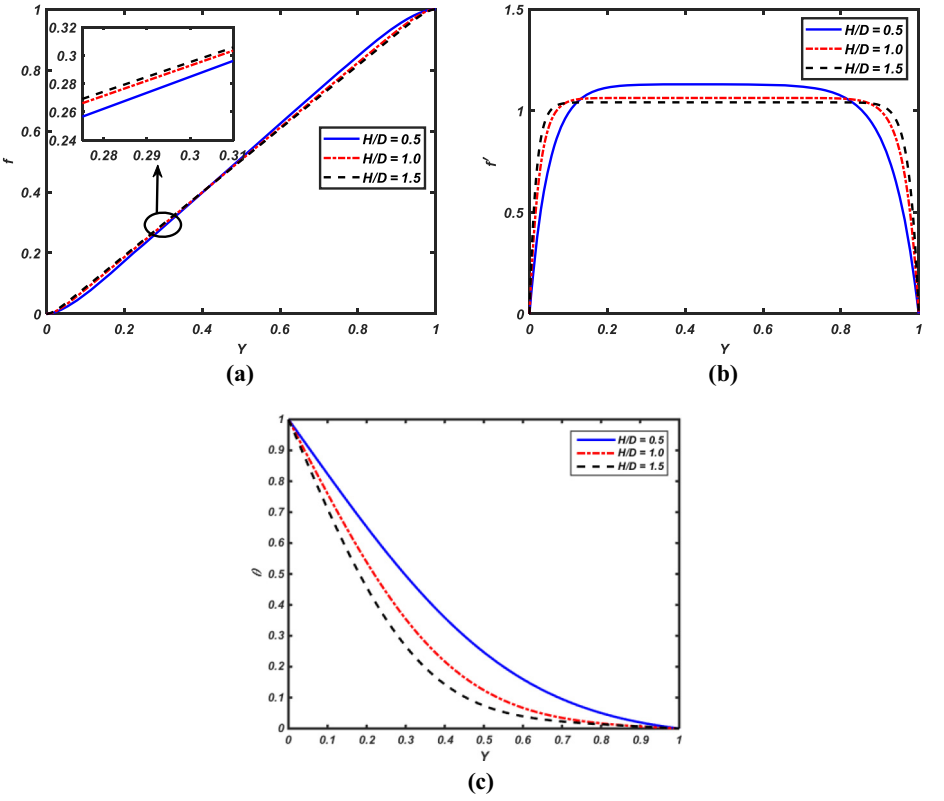

Figure 5.
Effect of Aspect ratio on: (a) f profile, (b) f' profile and (c) θ profile

Source: Figure by authors

temperature distribution within the system. With an increase in the Eckert number, the level of viscous dissipation grows, leading to an elevation in the temperature. This can be understood as the dissipation of mechanical energy of the fluid into thermal energy due to viscous effects. When the Eckert number is increased from 0 to 0.001, the temperature profile exhibits a slight increase. This indicates a small rise in the dissipation of mechanical energy and, subsequently, a minor temperature increase. However, as the Eckert number further increases from 0.001 to 0.01, a significant amplification in the temperature profile is observed. This suggests a more substantial contribution of viscous dissipation to the overall energy equation and a consequent rise in temperature. It is important to note that the variation in Eckert number does not have an impact on the velocity profiles since the viscous dissipation primarily influences the energy equation without affecting the momentum equation.

6.1.5 Porosity. Figure 8 provides insight into the variation of the dimensionless temperature and velocity profiles as porosity changes. Parts (a) and (b) of the figure reveal that changes in porosity have a relatively small effect on the velocity profiles of f and f'. The velocity profile of f shows a decreasing trend with increasing porosity, indicating a reduction in fluid flow velocity as the porosity of the medium increases. On the other hand,

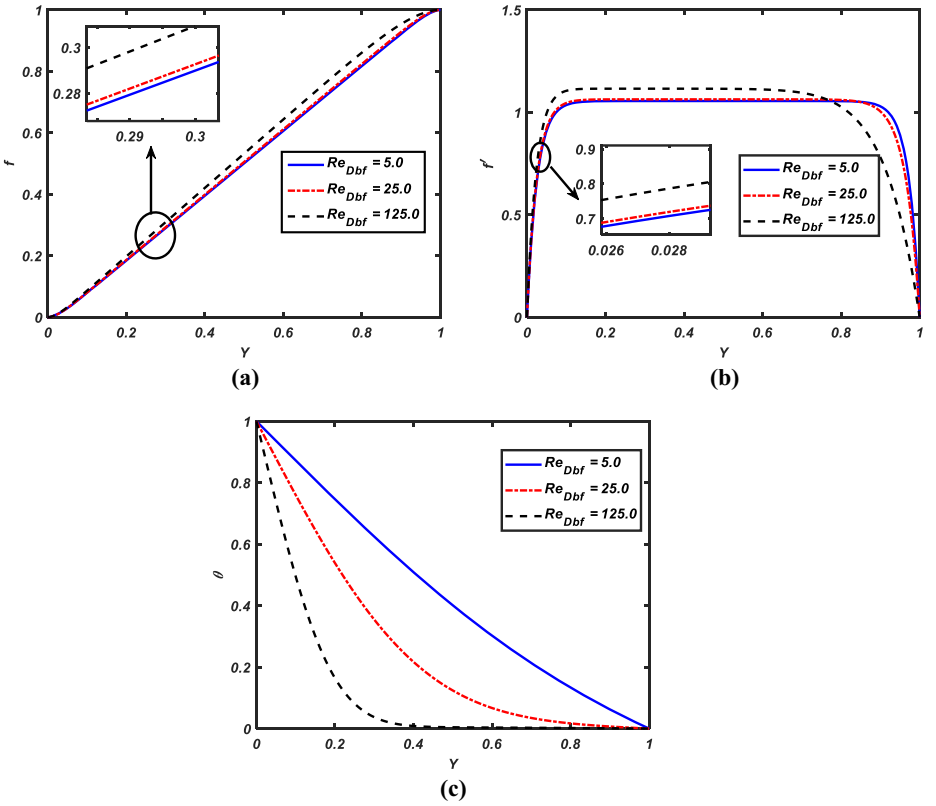

Figure 6.
Effect of Reynolds number on: (a) f profile, (b) f′ profile and (c) θ profile

Source: Figure by authors

the f' profile initially exhibits an increasing trend with porosity, followed by a subsequent decrease. This behavior suggests that the impact of porosity on the velocity profile is not linear and can vary depending on the specific conditions. Examining part (c) of Figure 8, it becomes apparent that the temperature profile has a negative correlation with porosity. This can be explained by considering equation (6) and the properties of the porous medium. In the equation, k_s represents the thermal conductivity of the solid matrix, while k_f corresponds to the effective thermal conductivity of the fluid-solid mixture within the porous medium. Since $k_s \gg k_f$, an increase in porosity leads to a decrease in the effective thermal conductivity of the mixture (k_{eff}). Consequently, the total thermal conductivity resistance increases, impeding heat transfer and resulting in a decrease in the temperature profile.

6.1.6 Hartmann number. Figure 9 illustrates the nondimensional velocity and temperature profiles as a function of the Hartmann number, which represents the effect of the magnetic field on these profiles. As the Hartmann number increases, the velocity profile of f in the proximity of the solid wall exhibits an increasing trend. This can be attributed to the magnetic field's influence on the fluid flow, which enhances the velocity near the wall. The magnetic field acts as a force that propels the fluid, resulting in an intensified flow in this region. However, in areas farther away from the wall, an opposite trend is observed,

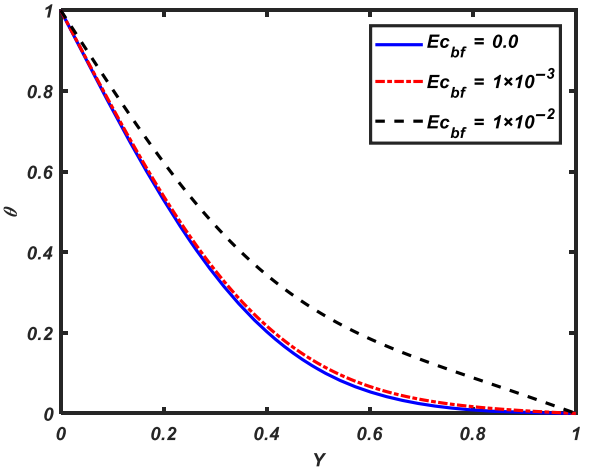

Figure 7.
Effect of Eckert number on θ profile

Source: Figure by authors

where an increase in the Hartmann number causes the velocity profile to dissipate. This phenomenon can be explained by the interplay between the magnetic field and the fluid dynamics, where the magnetic forces restrict and dampen the fluid motion as it moves away from the wall. Examining Figure 9(b) reveals that an increase in the Hartmann number induces considerable changes in the velocity profile of f'. Specifically, the maximum value of the velocity profile decreases as the Hartmann number increases, indicating the damping effect of the magnetic field on the fluid motion. Moreover, the velocity profile of f' becomes more uniform with increasing Hartmann number. In higher Hartmann numbers, the slope of the f' velocity profile near the wall and near the entrance of the heat sink becomes steeper, indicating the intensified impact of the magnetic field in those regions.

In Figure 9(c), the effect of the Hartmann number on the nondimensional temperature is shown. According to this figure, the Hartmann number does not have a significant impact on the nondimensional temperature distribution. This can be attributed to the fact that the primary influence of the magnetic field is on the fluid motion rather than the heat transfer process. While the magnetic field affects the velocity profiles, it has minimal impact on the temperature distribution, as the dominant heat transfer mechanisms are primarily governed by thermal conductivity and convective heat transfer.

6.1.7 Nanofluid volume fraction. Figure 10 shows the effects of nanofluid volume fraction variation on the nondimensional velocity and temperature profiles. Alterations in the volume fraction of nanoparticles added to the base fluid have inconsiderable impacts on the velocity and temperature profiles. When the volume fraction of nanoparticles increases, there is a decreasing trend observed in the profiles of f and f'. This can be attributed to the fact that the presence of nanoparticles in the fluid increases its viscosity, resulting in a slightly reduced fluid velocity. The higher viscosity creates additional resistance to fluid motion, leading to a slight decrease in the velocity profiles. However, in terms of temperature, an increase in the volume fraction of nanoparticles has an increasing effect (see Figure 10). This can be explained by the improved thermal conductivity of the nanofluid due to the presence of nanoparticles. The nanoparticles enhance the thermal conductivity of the base fluid, allowing for more efficient heat transfer. As a result, the temperature profile

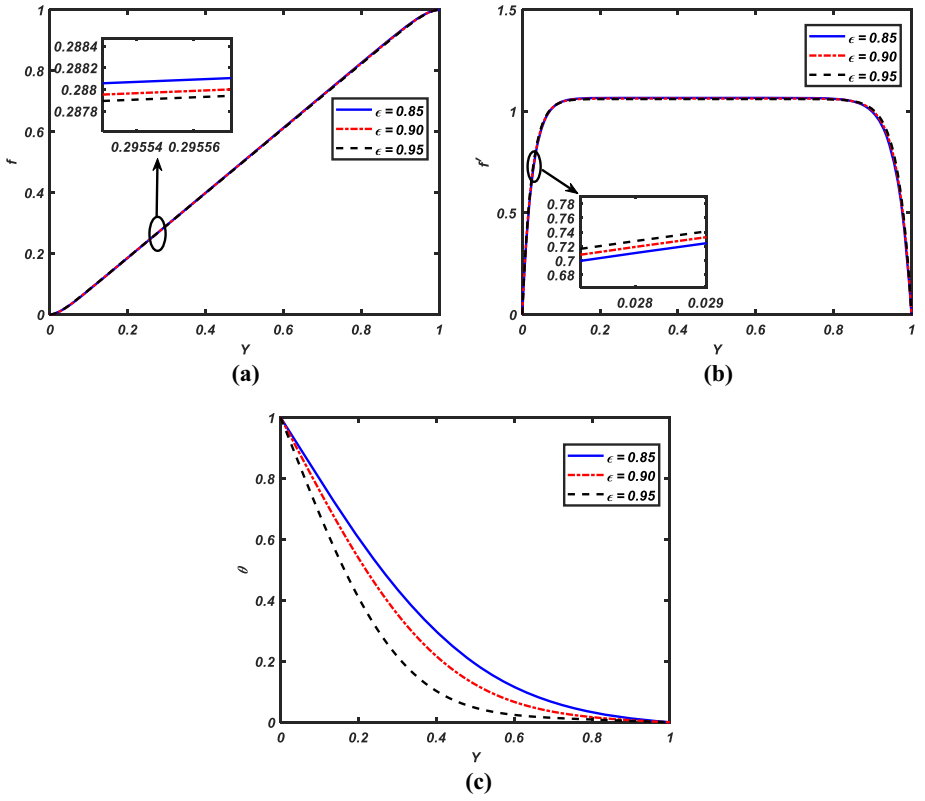

Figure 8.
Effect of porosity on: (a) f profile, (b) f′ profile and (c) θ profile

Source: Figure by authors

exhibits a slight increase with an increase in the volume fraction of nanoparticles. It is worth noting that while the variations in volume fraction have some influence on the temperature distribution, the impact on the velocity profiles is relatively small. The primary factor affecting the velocity profiles is the fluid viscosity, which is influenced by the presence of nanoparticles. On the other hand, the thermal conductivity enhancement provided by the nanoparticles plays a more significant role in determining the temperature distribution.

6.2 Thermal performance assessment

The effect of dimensionless numbers of Eckert, porosity, Darcy, Hartmann and aspect ratio on average Nusselt number has been explored in this part to look into the thermal performance of the fluid.

6.2.1 Eckert number. Figure 11 provides insight into the effect of the Eckert number on the thermal performance, specifically the Nusselt number, as a function of the Reynolds number. The Nusselt number, which characterizes the convective heat transfer, exhibits a positive correlation with the Reynolds number. This relationship can be justified by examining Figure 12, which focuses on the effect of the Eckert number and Reynolds number on the contours of temperature and stream function. In Figure 12, it is observed that

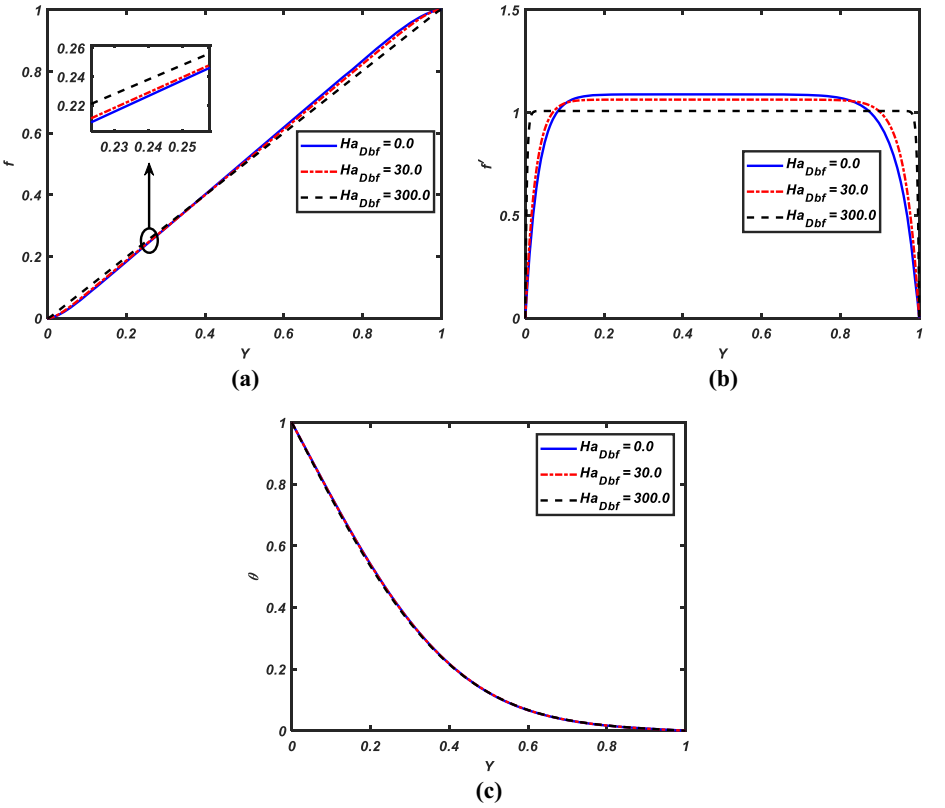

Figure 9.
Effect of Hartmann number on: (a) f profile, (b) f′ profile and (c) θ profile

Source: Figure by authors

an increase in the Reynolds number leads to an increase in the stream function contour. This indicates that a higher Reynolds number promotes greater fluid flow through the heat sink. As a result, more heat is transferred from the hot wall, leading to an increased temperature gradient in the regions surrounding the hot wall. This enhanced convective heat transfer contributes to an increase in the Nusselt number. On the other hand, the Eckert number plays a role in modifying the temperature distribution and, consequently, the Nusselt number. An increase in the Eckert number causes a decline in the temperature gradient. This reduction in the temperature gradient is attributed to the dissipation of energy due to viscous effects. Consequently, as the Eckert number increases, the Nusselt number decreases. It is important to note that the decrement in the Nusselt number is directly associated with the increase in the Eckert number. In other words, the amount of decreasing Nusselt number when Eckert number increases from 0.01 to 0.1 is greater than when Eckert number rises from 0 to 0.01. Furthermore, comparing the temperature contours in Figure 12 illustrates that effect of Eckert number in the lower Reynolds is greater than that of higher Reynolds.

6.2.2 Porosity. Figure 13 demonstrates the influence of porosity on thermal performance, as characterized by the Nusselt number. It is observed that as the porosity increases, the

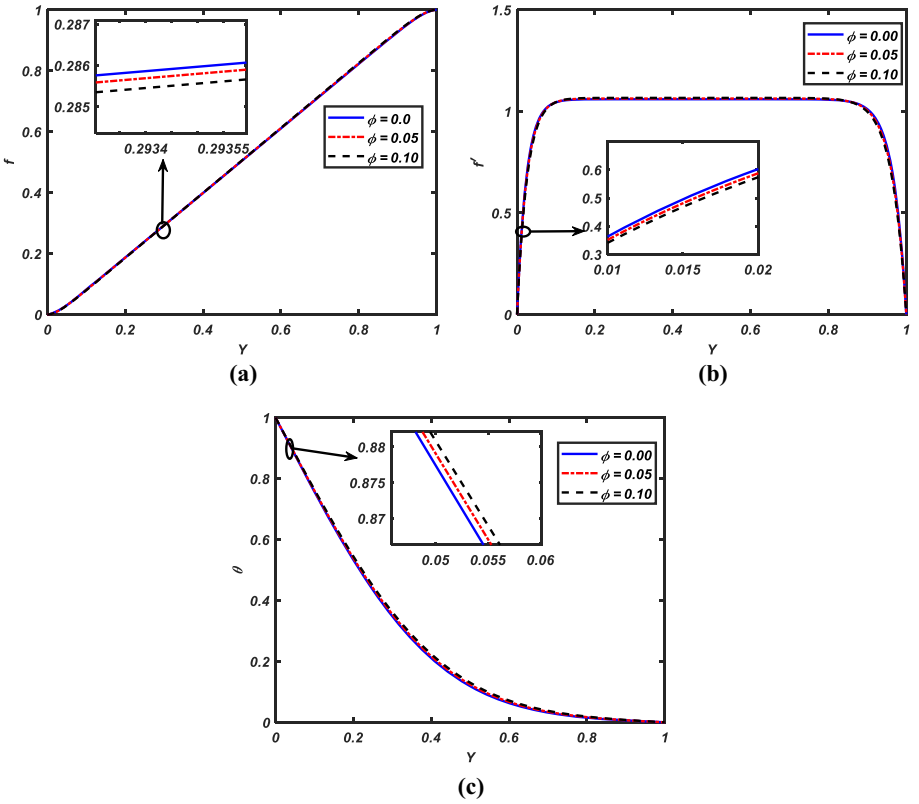

Figure 10.
Effect of nanofluid volume fraction on (a) f profile, (b) f′ profile and (c) θ profile

Source: Figure by authors

Nusselt number decreases. This decline in the Nusselt number can be attributed to the changes in thermal conductivity and heat transfer characteristics of the porous media. According to equation (6), the decrease in the Nusselt number can be understood by considering the effective thermal conductivity of the porous media, represented by the solid-phase thermal conductivity (k_s) and the effective thermal conductivity of the nanofluid (k_{nf}). In this case, the solid-phase thermal conductivity is much larger than the effective thermal conductivity of the nanofluid. As the porosity increases, the thermal conductivity coefficient (k_{eff}) decreases. This reduction in the thermal conductivity coefficient leads to an increase in the total thermal resistance within the porous media. Consequently, the heat transfer rate from the heat sink wall decreases, resulting in a decline in the Nusselt number.

6.2.3 Darcy number. Figure 14 illustrates the influence of the Darcy number on the Nusselt number as a function of the Reynolds number. As expected, an increase in the Darcy number (or an increase in permeability for a constant specific length) leads to a rise in the Nusselt number. This increase can be attributed to the enhanced slope of the nondimensional temperature profile due to the strengthening of the convection term [as observed in Figure 4(c)]. The higher Darcy number corresponds to a greater fluid flow rate through the porous medium, resulting in improved convective heat transfer. Consequently,

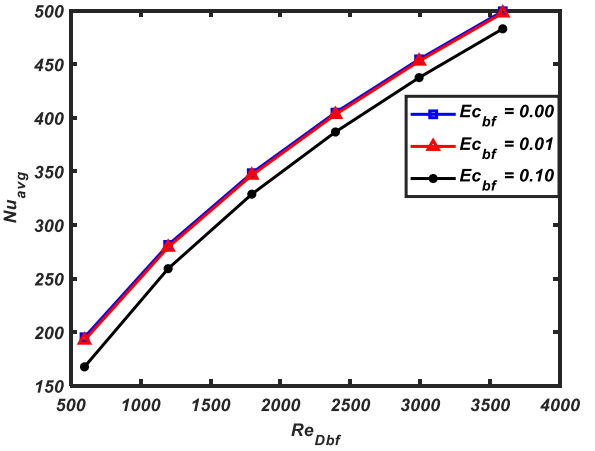

Figure 11.
Effect of Eckert number on Nusselt number as a function of Reynolds number

Source: Figure by authors

the Nusselt number, which quantifies the convective heat transfer, increases with increasing Darcy number. Moving on to Figure 15, it exhibits the effects of the Darcy number and porosity on the temperature and stream function contours. The Darcy number shows minimal influence on these contours, suggesting that it has a limited impact on the overall temperature distribution and flow patterns. The main driver for the temperature and flow behavior lies in other factors, such as the geometry, thermal properties and boundary conditions of the system. By comparing the temperature distribution contours at different porosity levels, it is observed that higher porosity values result in reduced heat conduction from the hot wall to the upper regions. This phenomenon arises due to the increased thermal resistance of the porous medium at higher porosities. The porous structure hinders the heat transfer process, leading to a lower rate of heat conduction.

6.2.4 Hartmann number. Figure 16 presents the impact of the Hartmann number on the Nusselt number as a function of the Reynolds number. It is observed that as the Hartmann number increases, there is a reverse relationship with the Nusselt number. In other words, higher Hartmann numbers are associated with lower Nusselt numbers. The decline in the Nusselt number with increasing Hartmann number is more significant at higher Reynolds numbers. At low Reynolds numbers, the effect of the Hartmann number on the Nusselt number is relatively small. The physical interpretation of this behavior can be attributed to the interaction between the magnetic field and the fluid flow. As the Hartmann number increases, the magnetic field becomes stronger, exerting a greater influence on the fluid motion. This, in turn, affects the convective heat transfer process. At low Reynolds numbers, the fluid flow is relatively weak, and the impact of the magnetic field is limited, resulting in a minor reduction in the Nusselt number. However, as the Reynolds number increases, the fluid flow becomes more dominant and the influence of the magnetic field becomes more significant. In this regime, an increase in the Hartmann number leads to substantial changes in the heat transfer characteristics. The stronger magnetic field alters the flow patterns and disrupts the convective heat transfer, resulting in a notable decrease in the Nusselt number.

6.2.5 Aspect ratio. Figure 17 illustrates the influence of the aspect ratio on the Nusselt number. It is observed that a decrease in the aspect ratio of the heat sink leads to an increase

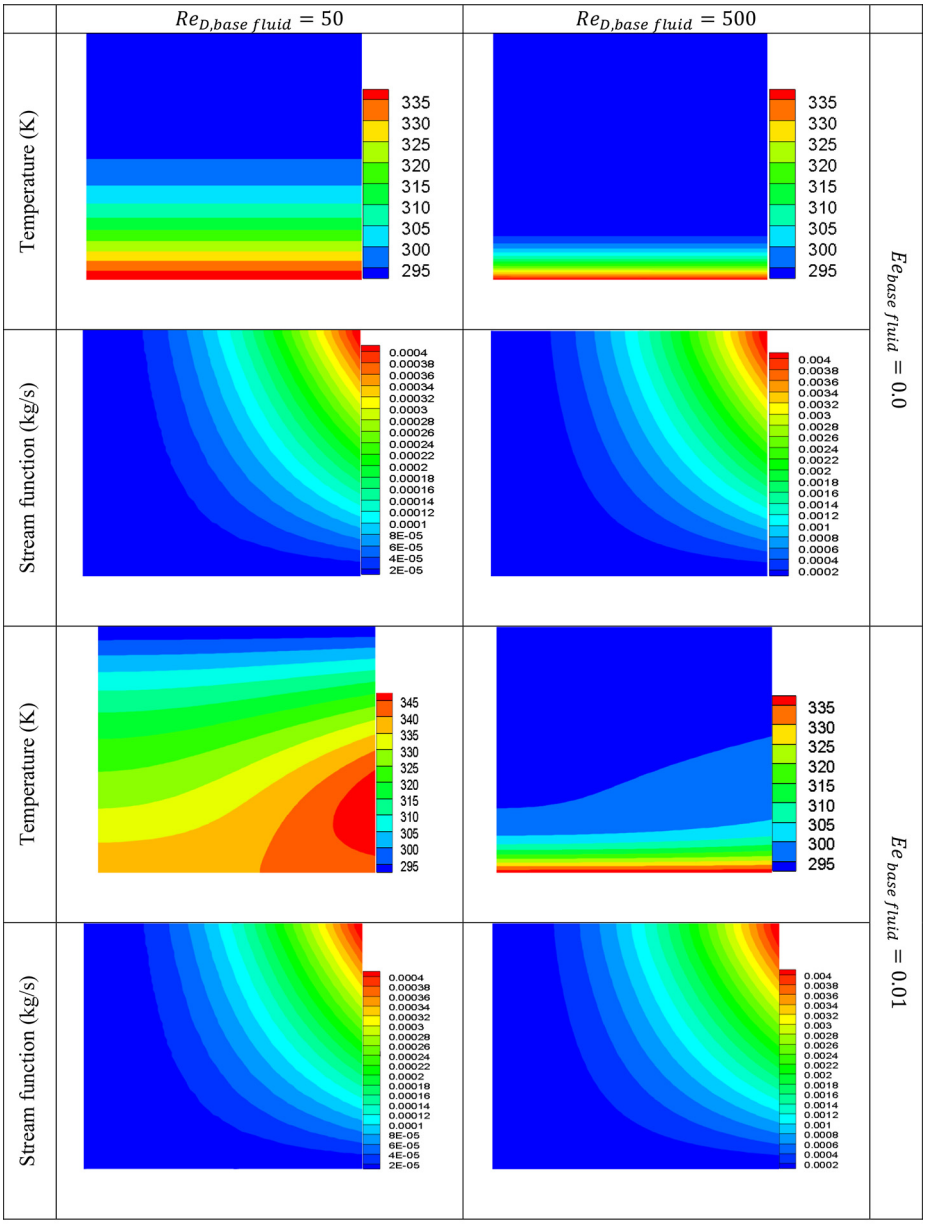

Source: Figure by authors

Figure 12.
Effect of Reynolds number and Eckert number on the stream function and temperature contours

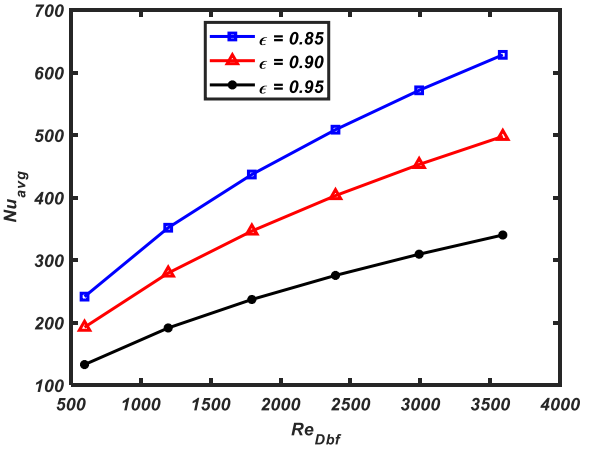

Source: Figure by authors

Figure 13.
Effect of porosity on Nusselt number as a function of Reynolds number

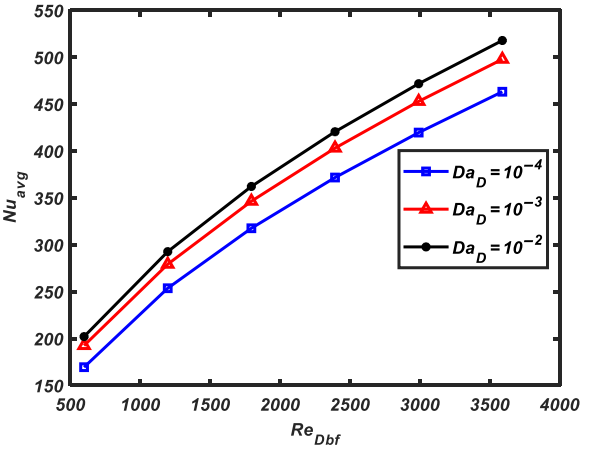

Source: Figure by authors

Figure 14.
Effect of Darcy number on Nusselt number as a function of Reynolds number

in the Nusselt number. This behavior can be attributed to the changes in the heat transfer characteristics resulting from the variation in aspect ratio. According to Figure 5(c), as the aspect ratio decreases, the heat sink becomes shorter relative to its width, which affects the thermal resistance of the heat sink. The increased thermal resistance impedes heat flow, resulting in higher temperature gradients and enhanced convective heat transfer. Consequently, the Nusselt number increases due to the improved heat transfer performance. Additionally, the comparison of temperature contours in Figure 18 reveals that changes in the Hartmann number have no significant effect on the temperature distribution. However, the increment of the Hartmann number alters the flow pattern within the system.

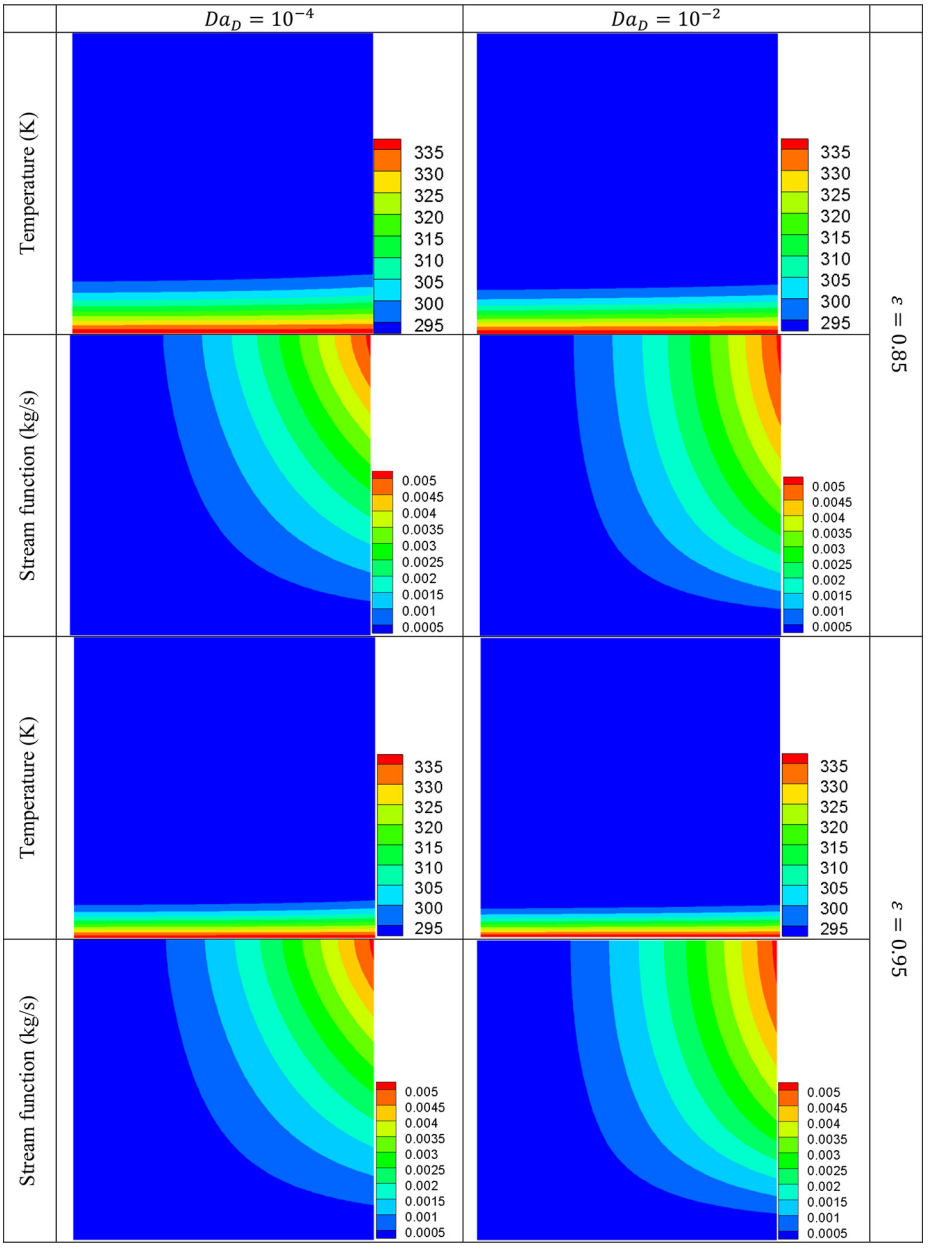

Source: Figure by authors

Figure 15.
Effect of Darcy number and porosity on temperature and stream function contour

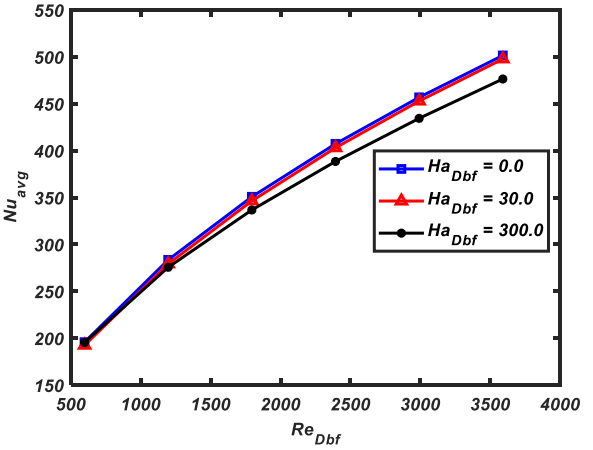

Figure 16.
Effect of Hartmann number on Nusselt number as a function of Reynolds number

Source: Figure by authors

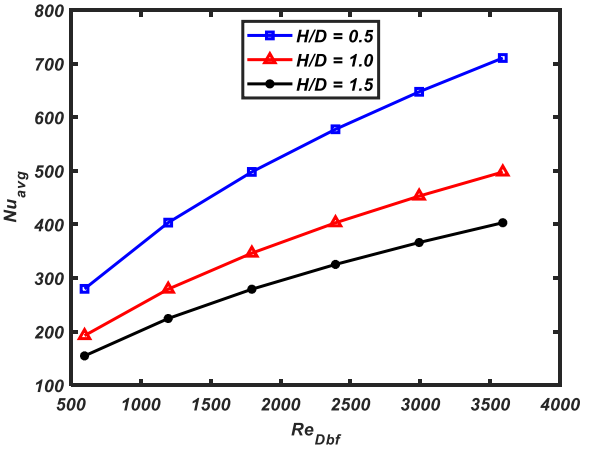

Figure 17.
Effect of aspect ratio on Nusselt number as a function of Reynolds number

Source: Figure by authors

Specifically, the curves of the streamline trajectories decrease, and the streamlines become more linear in shape. Moreover, the region with the highest temperature (red area) becomes smaller. This phenomenon is associated with the influence of the magnetic field, which modifies the flow behavior and redistributes the heat transfer within the system. The alteration in flow pattern affects the convective heat transfer and leads to changes in the Nusselt number. The findings highlight the importance of the aspect ratio in heat transfer performance. A lower aspect ratio, corresponding to a shorter heat sink, results in improved convective heat transfer and higher Nusselt numbers. Furthermore, the results emphasize the role of the Hartmann number in altering the flow pattern and streamlines. Although the

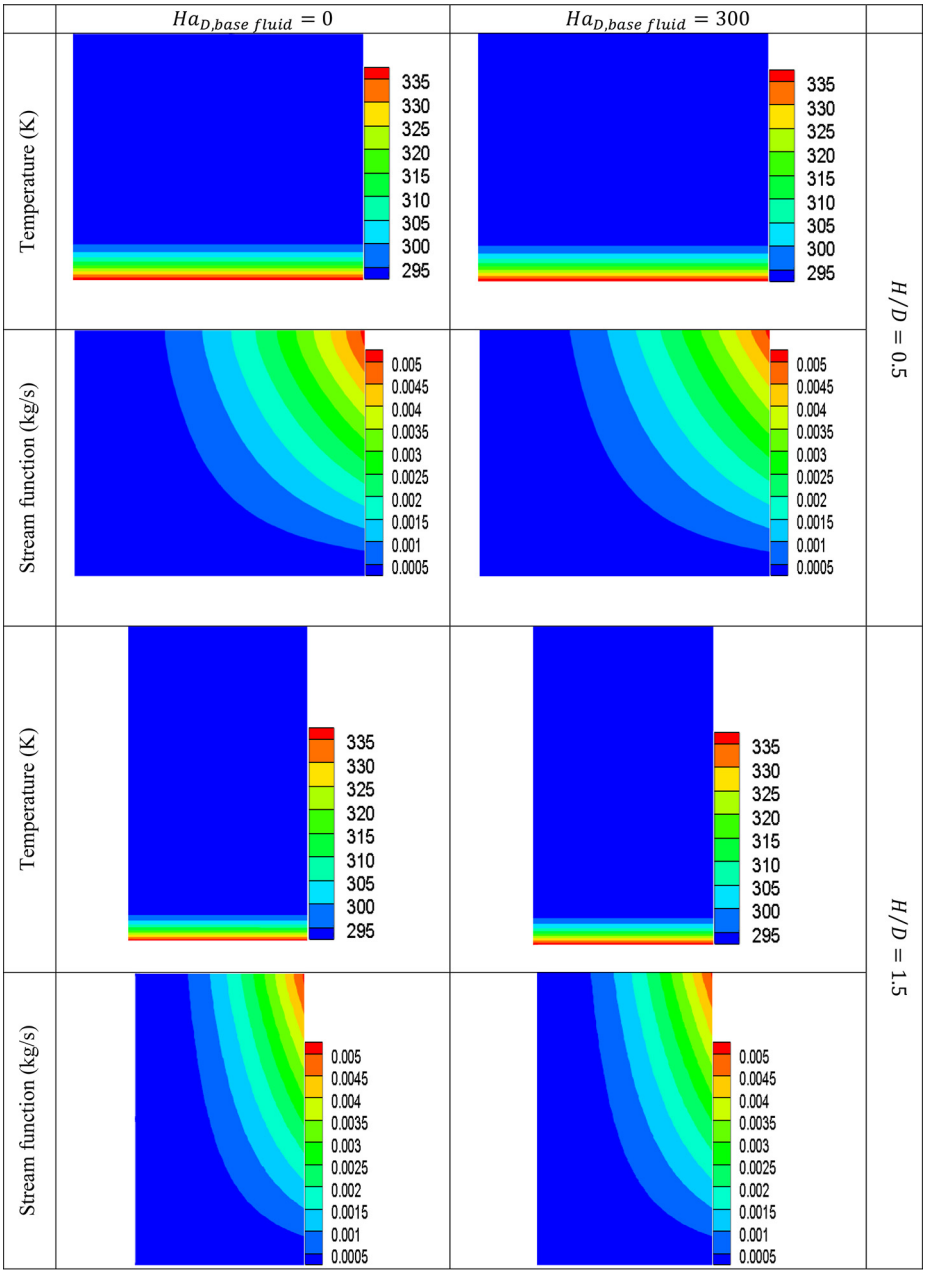

Source: Figure by authors

Figure 18.
Effects of aspect ratio and Hartman number on the temperature and stream function contours

effect on temperature distribution is minimal, the changes in flow behavior induced by the magnetic field have implications for heat transfer characteristics.

6.2.6 Nanofluid volume fraction. Figure 19 presents the investigations of the impact of nanofluid volume fraction on the Nusselt number as a function of the Reynolds number. The Reynolds number was varied within the range of 0 to 4,000, while three different nanofluid volume fractions were considered: 0, 0.05 and 0.1. This figure revealed that the Nusselt number exhibited minimal sensitivity to changes in nanofluid volume fraction. This outcome suggests that, within the specified Reynolds number range, the presence of nanoparticles in the fluid has a negligible effect on convective heat transfer. The lack of significant influence could be attributed to factors such as the size and concentration of nanoparticles, which may not have strongly interacted with the convective heat transfer mechanisms under consideration. Additionally, the thermal conductivity enhancement provided by the nanofluid at the examined volume fractions might have been inadequate to noticeably alter the heat transfer characteristics. These analytical findings contribute valuable insights into the role of nanofluid volume fraction on convective heat transfer and emphasize the need for further research, both analytical and experimental, to explore the influence of other factors, such as particle size, shape and concentration, particularly at higher Reynolds numbers. Additionally, it should be mentioned that adding nanofluid might be economically researched to see if it is effective.

7. Conclusion

In response to the growing concern over efficiently managing heat generated by modern electronic devices and computers, this study focused on the use of effective thermal solutions, specifically porous metal foams and cooling nanofluid. The objective was to investigate a cooling system capable of effectively dissipating CPU-generated heat. To achieve this, we used the Darcy–Brinkman–Forchheimer equations to account for the impact of a magnetic field on momentum, as well as the thermal equilibrium state equation to incorporate the effect of viscous dissipation on heat transfer.

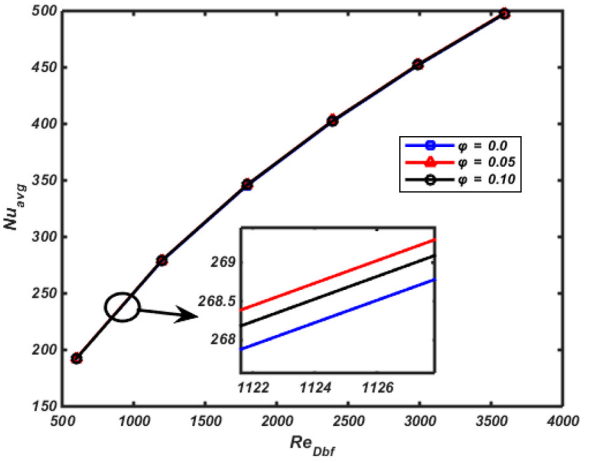

Source: Figure by authors

Figure 19.
Effect of nanofluid volume fraction on Nusselt number as a function of Reynolds number

Using numerical methods, we explored the intricate interactions between heat transfer and fluid flow within the system, ensuring the validity of our approach through meticulous validation procedures. Recent investigation aimed to comprehend the effects of various flow and geometric factors on flow behavior and heat transfer. Here are the key findings, along with their implications for thermal management and CPU cooling:

- In total, 45% and 46% decrease in Nusselt number at Reynolds numbers 600 and 3,500, respectively, with an increase in porosity from 0.85 to 0.95, while regarding porosity, there are no discernible changes in the velocity profile. This implies that higher porosity levels can significantly enhance heat dissipation efficiency within the system, crucial for preventing overheating in CPUs and electronic devices.
- The velocity profiles become more robust as the Darcy number rises. Moreover, going from a Darcy number of 10^{-4} to 10^{-2} improves the heat sink's thermal performance by 19.2% at Reynolds 600 and 11.8% at Reynolds 3,500. This finding emphasizes that increased fluid flow rates, achieved through higher Darcy numbers, contribute to more effective heat transfer, which is pivotal for maintaining optimal CPU functionality.
- The cooling fluid's temperature increases as the Eckert number rises from 0 to 0.1, although heat transfer decreases by 14.1% at Reynolds 600 and 3.3% at Reynolds 3,500. This highlights the complex interplay between fluid temperature and heat transfer rates, underscoring the need for careful consideration of fluid properties in thermal management strategies.
- Increasing the ratio of heat sink aspect ratio from 0.5 to 1.5 leads to a decrease in the velocity profile and decrease in the heat transfer rate by 44.7% at Reynolds 600 and 43.3% at Reynolds 3,500. This indicates that while altering the aspect ratio can influence fluid dynamics, it can also impact heat transfer efficiency, which is crucial for effective CPU cooling.
- The velocity profile decreases as the Hartmann number rises from 0 to 300. Moreover, it causes the heat sink's heat transfer rate to drop by 0.15% at Reynolds 600 and 5% at Reynolds 3,500. This finding highlights the potential of a magnetic field's influence on fluid flow and heat transfer, offering insights into novel ways to enhance thermal management strategies.

While these findings significantly contribute to thermal management understanding, acknowledging study limitations is crucial. External turbulence effects, real-world material variations and dynamic operational conditions were not fully considered, potentially impacting result accuracy. Simplifications and model assumptions could introduce errors.

Future work can expand the study's scope by incorporating intricacies like particle size distribution and nanofluid concentration, revealing nuanced heat transfer and fluid dynamics effects. Advanced models, such as the LTNE model, could enhance accuracy by addressing complexities overlooked by conventional models. Additionally, exploring a two-phase approach involving water and nanofluid offers insights into combined cooling techniques, potentially optimizing electronic device heat management through fluid interactions.

References

Akbar, N.S. and Khan, Z.H. (2015), "Influence of magnetic field for metachoronical beating of cilia for nanofluid with Newtonian heating", *Journal of Magnetism and Magnetic Materials*, Vol. 381, pp. 235-242.

Al-Rashed, M.H., Dzido, G., Korpyś, M., Smołka, J. and Wójcik, J. (2016), "Investigation on the CPU nanofluid cooling", *Microelectronics Reliability*, Vol. 63, pp. 159-165.

Aly, E.H. and Pop, I. (2019), "MHD flow and heat transfer over a permeable stretching/shrinking sheet in a hybrid nanofluid with a convective boundary condition", *International Journal of Numerical Methods for Heat and Fluid Flow*, Vol. 29 No. 9, pp. 3012-3038.

Bahiraei, M. and Heshmatian, S. (2017), "Application of a novel biological nanofluid in a liquid block heat sink for cooling of an electronic processor: thermal performance and irreversibility considerations", *Energy Conversion and Management*, Vol. 149, pp. 155-167.

Calmidi, V.V. and Mahajan, R.L. (2000), "Forced convection in high porosity metal foams", *Journal of Heat Transfer*, Vol. 122 No. 3, pp. 557-565.

Choi, J., Jeong, M., Yoo, J. and Seo, M. (2012), "A new CPU cooler design based on an active cooling heatsink combined with heat pipes", *Applied Thermal Engineering*, Vol. 44, pp. 50-56.

Dhahri, D., Slimi, K. and Nasrallah, S.B. (2010), "Viscous dissipation effects on heat transfer for oscillating flow in a pipe partially filled with a porous medium", *Comput Therm Sci An Int J*, Vol. 2 No. 4.

Do, K.H., Kim, T.H. and Kim, S.J. (2010), "Analytical and experimental investigations on fluid flow and thermal characteristics of a plate-fin heat sink subject to a uniformly impinging jet", *International Journal of Heat and Mass Transfer*, Vol. 53 Nos 9/10, pp. 2318-2323.

Feng, S.S., Kuang, J.J., Lu, T.J. and Ichimiya, K. (2015), "Heat transfer and pressure drop characteristics of finned metal foam heat sinks under uniform impinging flow", *J Electron Packag*, Vol. 137 No. 2, p. 21014.

Geridönmez, B.P. and Öztop, H.F. (2021), "Effects of partial magnetic field in a vented square cavity with aiding and opposing of MWCNT–water nanofluid flows", *Engineering Analysis with Boundary Elements*, Vol. 133, pp. 84-94.

Goodarzi, M., Tlili, I., Tian, Z. and Safaei, M.R. (2019), "Efficiency assessment of using graphene nanoplatelets-silver/water nanofluids in microchannel heat sinks with different cross-sections for electronics cooling", *International Journal of Numerical Methods for Heat and Fluid Flow*, Vol. 30 No. 1, pp. 347-372.

Gorzin, M., Ranjbar, A.A. and Hosseini, M.J. (2022), "Experimental and numerical investigation on thermal and hydraulic performance of novel serpentine minichannel heat sink for liquid CPU cooling", *Energy Reports*, Vol. 8, pp. 3375-3385.

Hajipour, M. and Dehkordi, A.M. (2012), "Analysis of nanofluid heat transfer in parallel-plate vertical channels partially filled with porous medium", *International Journal of Thermal Sciences*, Vol. 55, pp. 103-113.

Hosseini, S.R. and Sheikholeslami, M. (2019), "Investigation of the nanofluid convective flow and entropy generation within a microchannel heat sink involving magnetic field", *Powder Technology*, Vol. 351, pp. 195-202.

Huang, Z.F., Nakayama, A., Yang, K., Yang, C. and Liu, W. (2010), "Enhancing heat transfer in the core flow by using porous medium insert in a tube", *International Journal of Heat and Mass Transfer*, Vol. 53 Nos 5/6, pp. 1164-1174.

Hussain, M. and Sheremet, M. (2023), "Convection analysis of the radiative nanofluid flow through porous media over a stretching surface with inclined magnetic field", *International Communications in Heat and Mass Transfer*, Vol. 140, p. 106559.

Hussain, S., Mehmood, K. and Sagheer, M. (2016), "MHD mixed convection and entropy generation of water–alumina nanofluid flow in a double lid driven cavity with discrete heating", *Journal of Magnetism and Magnetic Materials*, Vol. 419, pp. 140-155.

Iqbal, J., Abbasi, F.M., Alkinidri, M. and Alahmadi, H. (2023), "Heat and mass transfer analysis for MHD bioconvection peristaltic motion of Powell-Eyring nanofluid with variable thermal characteristics", *Case Studies in Thermal Engineering*, Vol. 43, p. 102692.

Izadi, A., Abdipour, M. and Rasam, H. (2020a), "MHD forced convection of nanofluid flow in an open-cell metal foam heatsink under LTNE conditions", *Journal of Thermal Analysis and Calorimetry*, Vol. 141 No. 5, pp. 1847-1857.

Izadi, A., Siavashi, M., Rasam, H. and Xiong, Q. (2020b), "MHD enhanced nanofluid mediated heat transfer in porous metal for CPU cooling", *Applied Thermal Engineering*, Vol. 168, p. 114843.

Izadi, A., Siavashi, M. and Xiong, Q. (2019), "Impingement jet hydrogen, air and CuH2O nanofluid cooling of a hot surface covered by porous media with non-uniform input jet velocity", *International Journal of Hydrogen Energy*, Vol. 44 No. 30, pp. 15933-15948.

Khan, Z.H., Khan, W.A., Hamid, M. and Liu, H. (2020a), "Finite element analysis of hybrid nanofluid flow and heat transfer in a split lid-driven square cavity with Y-shaped obstacle", *Phys Fluids*, Vol. 32 No. 9.

Khan, Z.H., Khan, W.A., Haq, R.U., Usman, M. and Hamid, M. (2020b), "Effects of volume fraction on water-based carbon nanotubes flow in a right-angle trapezoidal cavity: FEM based analysis", *International Communications in Heat and Mass Transfer*, Vol. 116, p. 104640.

Khan, Z.H., Khan, W.A. and Pop, I. (2013), "Triple diffusive free convection along a horizontal plate in porous media saturated by a nanofluid with convective boundary condition", *International Journal of Heat and Mass Transfer*, Vol. 66, pp. 603-612.

Liu, D. and Garimella, S.V. (2005), "Analysis and optimization of the thermal performance of microchannel heat sinks", *International Journal of Numerical Methods for Heat and Fluid Flow*, Vol. 15 No. 1, pp. 7-26.

Mahesh, R., Mahabaleshwar, U.S., Aly, E.H. and Manca, O. (2023), "An impact of CNTs on an MHD Casson Marangoni boundary layer flow over a porous medium with suction/injection and thermal radiation", *International Communications in Heat and Mass Transfer*, Vol. 141, p. 106561.

Mohamad, A.A. (2003), "Heat transfer enhancements in heat exchangers fitted with porous media part I: constant wall temperature", *International Journal of Thermal Sciences*, Vol. 42 No. 4, pp. 385-395.

Mohebbi, R. and Rasam, H. (2020), "Numerical simulation of conjugate heat transfer in a square cavity consisting the conducting partitions by utilizing lattice Boltzmann method", *Physica A: Statistical Mechanics and Its Applications*, Vol. 546, p. 123050.

Naphon, P., Klangchart, S. and Wongwises, S. (2009), "Numerical investigation on the heat transfer and flow in the mini-fin heat sink for CPU", *International Communications in Heat and Mass Transfer*, Vol. 36 No. 8, pp. 834-840.

Nazari, M., Karami, M. and Ashouri, M. (2014), "Comparing the thermal performance of water, ethylene glycol, alumina and CNT nanofluids in CPU cooling: experimental study", *Experimental Thermal and Fluid Science*, Vol. 57, pp. 371-377.

Nield, D.A. and Kuznetsov, A.V. (2009), "The Cheng–Minkowycz problem for natural convective boundary-layer flow in a porous medium saturated by a nanofluid", *International Journal of Heat and Mass Transfer*, Vol. 52 Nos 25/26, pp. 5792-5795.

Odabaee, M., De Paepe, M., De Jaeger, P., T'Joen, C. and Hooman, K. (2013), "Particle deposition effects on heat transfer from a metal foam-wrapped tube bundle", *International Journal of Numerical Methods for Heat and Fluid Flow*, Vol. 23 No. 1, pp. 74-87.

Patankar, S. (1980), *Numerical Heat Transfer and Fluid Flow*, CRC Press. Taylor and Francis Group, LLC. FL, United States.

Pavel, B.I. and Mohamad, A.A. (2004), "An experimental and numerical study on heat transfer enhancement for gas heat exchangers fitted with porous media", *International Journal of Heat and Mass Transfer*, Vol. 47 No. 23, pp. 4939-4952.

Rasam, H., Roy, P., Savoldi, L. and Ghahremanian, S. (2020), "Numerical assessment of heat transfer and entropy generation of a porous metal heat sink for electronic cooling applications", *Energies*, Vol. 13 No. 15, p. 3851.

Reddy, Y.D. and Goud, B.S. (2023), "Comprehensive analysis of thermal radiation impact on an unsteady MHD nanofluid flow across an infinite vertical flat plate with ramped temperature with heat consumption", *Results in Engineering*, Vol. 17, p. 100796.

Rezazad Bari, A., Zabetian Targhi, M. and Heyhat, M.M. (2023), "A numerical study on thermo-hydraulic performance of micro pin-fin heat sink using hybrid pin-fins arrangement for electronic cooling devices", *International Journal of Numerical Methods for Heat and Fluid Flow*, Vol. 33 No. 7, pp. 2478-2508.

Sepasgozar, S., Faraji, M. and Valipour, P. (2017), "Application of differential transformation method (DTM) for heat and mass transfer in a porous channel", *Propulsion and Power Research*, Vol. 6 No. 1, pp. 41-48.

Sepehrnia, M., Khorasanizadeh, H. and Shafii, M.B. (2021), "Effect of transverse and parallel magnetic fields on thermal and thermo-hydraulic performances of ferro-nanofluid flow in trapezoidal microchannel heat sink", *International Journal of Numerical Methods for Heat and Fluid Flow*, Vol. 31 No. 7, pp. 2089-2111.

Shampine, L.F., Kierzenka, J. and Reichelt, M.W. (2000), "Solving boundary value problems for ordinary differential equations in MATLAB with bvp4c", *Tutor Notes*, Vol. 2000, pp. 1-27.

Sheikholeslami, M. (2018), "Influence of magnetic field on Al2O3-H2O nanofluid forced convection heat transfer in a porous lid driven cavity with hot sphere obstacle by means of LBM", *Journal of Molecular Liquids*, Vol. 263, pp. 472-488.

Sheikholeslami, M. and Ganji, D.D. (2016), "Nanofluid convective heat transfer using semi analytical and numerical approaches: a review", *Journal of the Taiwan Institute of Chemical Engineers*, Vol. 65, pp. 43-77.

Sheikholeslami, M., Hatami, M. and Ganji, D.D. (2013), "Analytical investigation of MHD nanofluid flow in a semi-porous channel", *Powder Technology*, Vol. 246, pp. 327-336.

Siavashi, M., Rasam, H. and Izadi, A. (2019), "Similarity solution of air and nanofluid impingement cooling of a cylindrical porous heat sink", *Journal of Thermal Analysis and Calorimetry*, Vol. 135 No. 2, pp. 1399-1415.

Xu, H., Gong, L., Huang, S. and Xu, M. (2015), "Flow and heat transfer characteristics of nanofluid flowing through metal foams", *International Journal of Heat and Mass Transfer*, Vol. 83, pp. 399-407.

Corresponding author
Hamed Rasam can be contacted at: hamed.rasam@polito.it